Importance of isomerization reactions for the OH radical regeneration from the photo-oxidation of isoprene investigated in the atmospheric simulation chamber SAPHIR

Anna Novelli[1], Luc Vereecken[1], Birger Bohn[1], Hans-Peter Dorn[1], Georgios I. Gkatzelis[1,2,3], Andreas Hofzumahaus[1], Frank Holland[1], David Reimer[1], Franz Rohrer[1], Simon Rosanka[1], Domenico Taraborrelli[1], Ralf Tillmann[1], Robert Wegener[1], Zhujun Yu[1,2], Astrid Kiendler-Scharr[1], Andreas Wahner[1] and Hendrik Fuchs[1]

[1]Forschungszentrum Jülich, Institute for Energy and Climate Research: Troposphere (IEK-8), 52425 Jülich, Germany
[2]now at: NOAA Earth Systems Research Laboratory, Boulder, Colorado 80305, United States
[3]now at: Cooperative Institute for Research in Environmental Sciences, Boulder, Colorado 80309, United States
[4]now at: Institute of Mass Spectrometry and Atmospheric Environment, Jinan University, Guangzhou 510632, China

Correspondence to: Anna Novelli (a.novelli@fz-juelich.de)

Supporting information

Table of content

A Theoretical work

A.1 Isoprene di-HPCARP-RO_2-I

A 1.1 Methodology

The reactants, transition states and products in the studied mechanistic branches of the isoprene chemistry were characterized at the M06-2X and CCSD(T) levels of theory. A brute force search of the conformer space for each of these structures was performed at the M06-2X/cc-pVDZ level of theory,(Dunning, 1989; Zhao and Truhlar, 2008; Alecu et al., 2010; Bao et al., 2017) starting from a systematic series of starting geometries generated by orienting the internal rotors along a set of dihedral angles reasonable for the type of rotor, and optimizing the geometry. While there is no guarantee that this approach yields all stable conformers, it should provide a near-complete description of the rotameric space. For the case at hand, ~24000 distinguishable structures were located from ~60000 starting geometries. The most relevant conformers (~850 structures across all reactions examined) were then fully re-optimized at the M06-2X/aug-cc-pVTZ level of theory.(Dunning, 1989) The number of conformers re-optimized at this higher level of theory differs per structure (see Table S1), but enough were included to cover over ~80% of the thermal population at 300K. Intrinsic reaction coordinate (IRC) calculations were performed on the lowest transition states (TS) to verify the nature to the transition state; the end points of these trajectories were further optimized and the energies used for determining an Eckart energy barrier shape. Finally, single energy point calculations at the CCSD(T)/aug-cc-pVTZ level of theory (Purvis and Bartlett, 1982) were performed on the energetically lowest-lying geometries of each structure, to further refine the energy barrier estimates.

The rate coefficients are calculated using multi-conformer canonical transition state theory (MC-CTST), where each structure is described as the ensemble of each of its conformers in a rigid rotor, harmonic oscillator approximation (Vereecken and Peeters, 2003).

$$k(T) = \frac{kT}{h}\frac{\kappa \cdot Q^{\neq}(T)}{Q_{reactant}(T)} exp\left(\frac{-E_b}{kT}\right) \qquad \text{(eq. S1)}$$

The barrier height E_b is the ZPE-corrected energy difference between the lowest conformers of transition state and reactant. The partition functions for each critical point is obtained from a Boltzmann-weighted sum of the partition functions $Q_i(T)$ of the n_{conf} conformers constituting that critical point, with $E_i = 0$ for the lowest-energy conformer:

$$Q(T) = \sum_{i=1}^{n_{conf}} Q_i\,(T) \cdot exp\left(\frac{-E_i}{kT}\right) \qquad \text{(eq. S2)}$$

This relies on a (near-)Boltzmann equilibrium population across all conformers, e.g. by internal rotation being significantly faster than chemical transformation reactions, a condition easily fulfilled for the reaction examined, given the much higher energy barriers for chemical reaction. To improve the prediction of k(T) and its temperature dependence, the partition functions $Q(T)^{all}$ are estimated for the M06-2X/aug-cc-pVTZ level of theory by combining the high level M06-2X/aug-cc-pVTZ result, available for the dominant conformers, with the low-level M06-2X/cc-pVDZ rovibrational characteristics, available for all conformers, as follows:

$$Q(T)_{high}^{all} = Q(T)_{high}^{selected} \times \frac{Q(T)_{low}^{all}}{Q(T)_{low}^{selected}} \quad \text{(eq. S3)}$$

i.e. the full partition function at the M06-2X/aug-cc-pVTZ level of theory is estimated by scaling the partition function for the dominant conformers to the total population, using the M06-2X/cc-pVDZ information of the minor conformers scaled to higher-level M06-2X/aug-cc-pVTZ. This procedure mitigates most of the impact of omitting the higher-energy conformers at the more costly levels of theory, and provides an approach that can be systematically improved to the limit of full characterization at the higher level of theory. Alternative additive schemes for merging of the high- and low levels of theory, e.g. the following:

$$Q(T)^{all} = Q(T)_{high}^{selected} + Q(T)_{low}^{all} - Q(T)_{low}^{selected} \quad \text{(eq. S4)}$$

were not retained, as such additive schemes do not scale the low-level conformer partition functions to the high-level properties, and thus converge somewhat slower to the limit where all conformers are treated at the high level of theory. Tunneling, κ, is accounted for by asymmetric Eckart tunneling, where the conformer-specific reactant and product energies, and imaginary wavenumber, of the lowest-lying TS conformer are used in the calculation. As the modeling study shows that the chemistry is not overly sensitive to the exact rate coefficient, we saved some computational cost at this time by not implementing conformer-specific tunneling κ_i in $Q^{\neq}(T)$ (e.g. Ocana et al., 2019(Ocaña et al., 2019)) but applying the same tunneling correction κ to all conformers. Conformer-specific tunneling will be implemented later when merging the current data into a structure-activity relationship (SAR).

As shown below, the rates of fast H-scrambling exceed the rates of product formation by 3 to 4 orders of magnitude, instating a fast equilibrium between **di-HPCARP-RO$_2$-Ia**, **-Ib**, and **-Ic**. In the absence of other loss processes that approach the rate of H-scrambling (as would be the case in e.g. high concentrations of NO, HO_2 or RO_2 radicals), one can then calculate a bulk rate coefficient for aldehyde H-migration, forming the tri-hydroperoxy-acyl radical. Within the MC-TST paradigm, this involves calculating the partition functions in eq. S1 across all **di-HPCARP-RO$_2$-I** and all aldehyde-H-shift TS conformers, as follows:

$$Q_{reactant}(T) = \sum_{j=a,b,c} \sum_{i=1}^{n_{conf\,j}} Q_{\text{di-HPCARP-RO2-I}j,i}(T) \cdot exp\left(\frac{-E_{\text{di-HPCARP-RO2-I}j,i}}{kT}\right) \quad \text{(eq. S5)}$$

$$Q^{\neq}(T) = \sum_{j=1,4;1,5;1,6} \sum_{i=1}^{n_{conf\,j}} Q^{\neq}_{j\text{-aldehyde-H-shift},i}(T) \cdot exp\left(\frac{-E_{\text{TS}j,i}}{kT}\right) \quad \text{(eq. S6)}$$

where $E_{\text{diHPCARP\_I}j,i}$ is the energy of the i-th conformer of **di-HPCARP-RO$_2$-I*j*** (j=a,b,c) relative to the lowest **di-HPCARP-RO$_2$-I** conformer, and $E_{TSj,i}$ the energy of the i-th conformer of the 1,4-, 1,5-, and 1,6-aldehyde-H-shift relative to the lowest aldehyde-H-shift TS conformer, while $Q_{\text{di-HPCARP-RO2-I}\,j,i}(T)$ and $Q^{\neq}_{j\text{-aldehyde-H-shift},i}$ are the conformer-specific partition functions; $n_{conf\,j}$ signifies the number of conformers for structure j. The overall barrier E_b in eq. S1 is then the (ZPE-corrected) energy difference between the lowest **diHPCARP-RO$_2$-I** conformer and the lowest aldehyde-H-shift TS conformer (in this case, the lowest-energy **diHPCARP-RO$_2$-Ic** and 1,6-aldehyde-H-shift conformers). The rate coefficients calculated thus are included in Table 3. Note that H-scrambling does not alter the stereo-specificity, i.e. eq. S5 and S6 must be calculated for each stereo-specific pool of reactants/TS. In the current case, the

difference in reaction rate between the two isomeric pools is not overly large, and a generalized expression can be obtained by averaging the two stereo-specific rate coefficients (see Table S1).

A 1.2 Reaction mechanism for di-HPCARP peroxy radicals

Table S1 shows a summary of the quantum chemical analysis of the **di-HPCARP-RO_2-I** system. These molecules have 2 chiral carbon atoms, where (2R,3R) and (2S,3S) enantiomers have identical rovibrational data, with a second distinct set of data for the (2R,3S) and (2S,3R) enantiomers. For some reactions the energetic differences are slight, but barrier height differences of several kcal mol^{-1} exist for H-migration reactions spanning across both chiral atoms, owing to the impact on ring strain and substituent interaction in the cyclic TS.

Formation of acyl radicals by migration of the aldehyde H-atom is an accessible channel for all **di-HPCARP-RO_2-I** isomers; the barrier height depends strongly on the TS cycle size, and changes from over 20 kcal mol^{-1} for a 1,4-aldehyde-H-migration, to as low as 16.3 kcal mol^{-1} for a 1,6-aldehyde-H-migration. The energetically most favorable H-migrations, however, are those involving migration of H-atoms of the hydroperoxide groups to the peroxy radical site, which allows rapid scrambling of the H-atoms, thus allowing access to reaction channels inaccessible from **di-HPCARP-RO_2-Ia** formed initially from **Z-δ-RO_2-I** (see main paper). The reactions of the **di-HPCARP-RO_2-II** isomers can be expected to be similar, i.e. fast hydroperoxide H-scrambling with energy barriers several kcal mol^{-1} below the aldehyde-H-migration pathways. Our results are analogous to those of Møller et al. (2019) (see also below).

HO_2 elimination is found to have too high barriers to compete (see Table S1 and 2), and is not studied in great detail. HO_2 elimination with a $–CH_3$ H-atom is omitted as this is expected to be even less favorable than those with aldehyde- or α-OOH H-atoms owing to the stronger C–H bond. 1,4- and 1,5-migration of the H-atoms from an -OOH-substituted carbon in **di-HPCARP-RO_2-I** is found to be less favorable than shifting the aldehyde-H-atom; while the energy barrier for the α-OOH 1,5-H-shift is only slightly higher than for the 1,4-aldehyde-H-migration, the additional entropic disadvantage of losing an additional degree of internal rotation in the TS lowers the rate coefficient significantly (see Table S1). While HO_2 elimination and α-OOH H-migrations were only examined for **di-HPCARP-RO_2-Ia**, the H-scrambled forms **-Ib** and **-Ic** are not expected to present more favorable channels for these reaction classes, as no pathways exist with more weakly bonded H-atoms, nor allowing for a TS with a lower ring strain. Likewise, it is improbable that **di-HPCARP-RO_2-II** isomers, which differ only by the position of the $-CH_3$ group, show channels that are competitive against the aldehyde- and hydroperoxide-H-migrations discussed above.

Table S1: Relative energies (kcal mol^{-1}) of the reactants and transition states for the stereo-specific chemistry of di-HPCARP-RO$_2$-I (2-Me-3,4-diOOH-butanal-2-peroxyl), at the CCSD(T)/aug-cc-pVTZ//M06-2X/aug-cc-pVTZ level of theory. Also indicated are the number of distinguishable conformers characterized at the different levels of theory, and the fraction of the population covered by the data at the highest level of theory.

Reaction	E_{rel}	# Conformers [a]	Pop. fraction [b]
(*2R,3R*)-2-Me-3,4-diOOH-butanal-2-peroxyl (**A**)	0.0	64 / 1470	0.91
1,4-aldehyde-H-migration	21.4	24 / 251	0.88
1,4-α-OOH-H-migration	28.6	6 / 125	0.98
1,5-α-OOH-H-migration	22.6	22 / 212	0.96
1,6-OOH-H-migration to **B**	19.3	6 / 100	0.88
1,7-OOH-H-migration to **C**	12.3	14 / 35	0.99
Aldehyde-HO$_2$-elimination	29.4[c]	[d]	
α-OOH-HO$_2$-elimination	31.9[c]	[d]	
(*2R,3R*)-2-Me-2,4-diOOH-butanal-3-peroxyl (**B**)	0.6	47 / 1290	0.83
1,5-aldehyde-H-migration	18.5	18 / 146	0.95
1,6-OOH-H-migration to **C**	18.9	33 / 95	0.99
(*2R,3R*)-2-Me-2,3-diOOH-butanal-4-peroxyl (**C**)	-1.2	39 / 1234	0.96
1,6-aldehyde-H-migration	17.6	27 / 157	0.97
(*2R,3R*)-2-Me-2,3,4-diOOH-1-oxo-1-butyl (**D**)	3.4	82 / 2719	0.79
CO elimination	11.1	104 / 2335	0.83
(*2R,3S*)-2-Me-3,4-diOOH-butanal-2-peroxyl (**A'**)	0.0	26 / 1362	0.87
1,4-aldehyde-H-migration	20.6	25 / 253	0.96
1,4-α-OOH-H-migration	27.2	4 / 128	0.99
1,5-α-OOH-H-migration	23.0	27 / 215	0.98
1,6-OOH-H-migration to **B'**	16.4	9 / 74	0.99
1,7-OOH-H-migration to **C'**	14.2	14 / 60	0.99
Aldehyde-HO$_2$-elimination	29.3[c]	[d]	
α-OOH-HO$_2$-elimination	31.3[c]	[d]	
(*2R,3S*)-2-Me-2,4-diOOH-butanal-3-peroxyl (**B'**)	-1.5	40 / 1280	0.91
1,5-aldehyde-H-migration	19.4	24 / 157	0.93
1,6-OOH-H-migration to **C'**	18.9	17 / 99	0.96
(*2R,3S*)-2-Me-2,3-diOOH-butanal-4-peroxyl (**C'**)	-1.3	46 / 1172	0.94
1,6-aldehyde-H-migration	16.3	25 / 146	0.98
(*2R,3S*)-2-Me-2,3,4-diOOH-1-oxo-1-butyl (**D'**)	3.1	65 / 2904	0.83
CO elimination	10.8	68 / 2495	0.78
2,2,2-triMe-acetyl	0.00		
CO elimination	9.66		
O$_2$ addition	0.47		
2,2,2-triMe-acetylperoxy	-32.80		
2,2-diMe-2-OOH-acetyl	0.00		
CO elimination	7.83		
O$_2$ addition	0.63		
2,2-diMe-2-OOH-acetylperoxy	-31.31		

[a] Number of distinguishable conformers found, with the last number indicating all conformers characterized at the M06-2X/cc-pVDZ level of theory, and the number before the dividus the number of conformers re-optimized at the M06-2X/aug-cc-pVTZ level of theory. [b] Fraction of the population at 300K that is based on M06-2X/aug-cc-pVTZ rovibrational data. The remainder of the population is described by scaling the partition function at the M06-2X/cc-pVDZ level towards the aug-cc-pVTZ data (see methodology section). [c] Energy barrier at the M06-2X/aug-cc-pVTZ level of theory. [d] The conformational space is not examined in as much detail as the other structures; statistics are omitted.

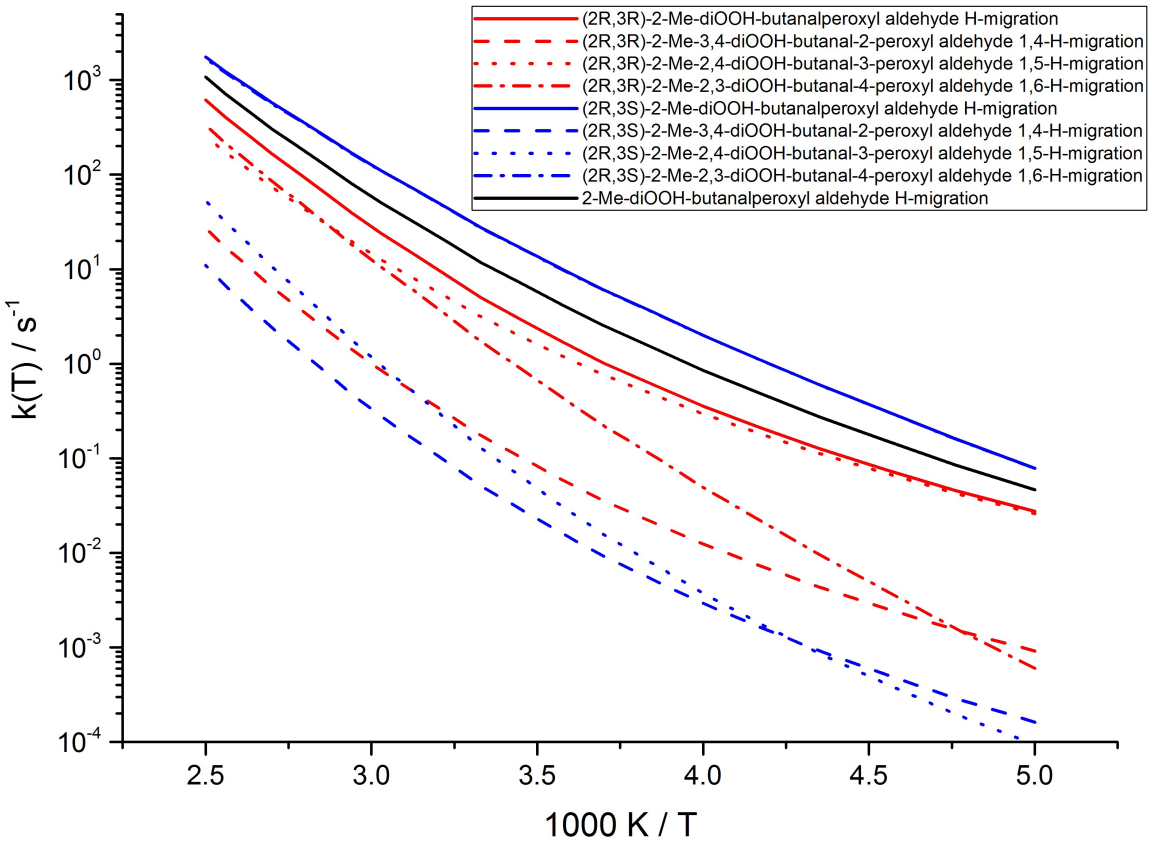

Figure S1: Temperature-dependent rate coefficients for the aldehyde H-shift in di-HPCARP-RO_2-I.

A 1.3 Comparison to literature theoretical data

There are two recent theoretical kinetic studies available examining the di-HPCARP-RO_2-I chemical system. A detailed comparison of the methodological differences is technical, and outside the scope of the current paper. To assess the uncertainties of the predictions, however, it is useful to give a short comparison of the results. We limit ourselves here to a discussion of the (R,R)-conformers, though the comparison can be generalized.

The first study by Wang et al. (2018) identified 9 conformers for di-HPCARP-RO_2-Ia, and 9 conformers for the transition state for 1,4-aldehyde-H-migration, from an examination of a subset of the conformational space with a selection of conformers based on semi-empirical methods. Despite the limited set of conformers, the rate coefficient at 298K, 0.86 s^{-1}, is only a factor 1.3 below our predicted rate of 1.15 s^{-1} based on all conformers. It is unclear whether this accuracy is due to fortuitous cancellation of error, or from judicious selection of the two (out of 8) degrees of freedom for internal rotation considered; note that the authors state that all 9 di-HPCARP-RO_2-Ia conformers can undergo the 1,4-aldehyde-H-migration directly, which indicates they include some less stable conformers, as our set of 9 energetically lowest conformers includes structures where the aldehyde H-atom and the radical oxygen

are not pointing towards each other. We optimized some of the provided conformers at the M06-2X/cc-pVDZ level of theory, finding them to be up to 8.7 kcal mol^{-1} above our most stable conformer, indicating that at least some of the 9 conformers have a negligible contribution to the thermal population. For the 1,5-α-OOH-H-migration, this study finds a rate coefficient 9.2×10^{-1} s^{-1}, over an order of magnitude higher than our value of 5×10^{-3} s^{-1}, mostly due to their reported barrier height being several kcal mol^{-1} below our value; these results are again likely distorted due to the strongly reduced conformer space missing low-energy conformers. Wang et al. (2018) do not examine any of the other aldehyde H-migration pathways to allow further comparison. The barrier for CO elimination after aldehyde H-migration, 8.5 kcal mol^{-1}, somewhat higher than our value which, combined with the limited set of conformers considered, results in a slower dissociation rate of 6.6×10^{6} s^{-1} compared to our value of 2×10^{8} s^{-1}. For such low values of CO elimination barrier heights, O_2 addition forming acylperoxy radicals would become competitive.

The methodology used by Møller et al. (2019) is more directly comparable to our methodology, and includes an extensive search of the conformer space, while the ROCCSD(T)-F12a/cc-pVDZ-F12//ωB97X-D/aug-cc-pVTZ level of theory used for the rovibrational and energetic parameters in the multi-conformer kinetics is of a comparable class of methods as the methodology used in our work. In most cases, we find strongly comparable barrier heights, with differences of a few tenths of a kcal mol^{-1} only, as expected from the levels of theory applied. Despite these resemblances, the predicted rate coefficients still differ by over an order of magnitude at room temperature. We surmise that these differences are caused by the low-level methodology used to discover and screen the conformers as outlined in Møller et al. (2016), which returns only a subset of the conformers. For example, Møller et al. (2019) report finding over 600 conformers for R,R-di-HPCARP-RO_2-Ia, whereas we have characterized almost 1500 conformers for this compound, over twice as many. Their semi-empirical screening might hope to find predominantly the most important, lowest-energy conformers, where the ~800 missed conformers would then be almost exclusively unstable, high-energy conformers with negligible contribution to the population. However, Møller et al. (2019) found 11 conformers below a 2 kcal mol^{-1} cutoff, whereas we found 27 conformers below 2 kcal mol^{-1} (M06-2X/aug-cc-pVTZ level of theory), indicating that low-energy conformers are missed in about equal proportion as for the total conformer pool. The 11 lowest conformers in our subset of 27 contribute less than 50 % of the thermal population at 300K, thus not describing the population all that well; it is unclear if the 11 conformers of Møller et al. (2019) actually correspond to our lowest 11. Furthermore, while the use of an energetic cut-off (typically 2 kcal mol^{-1} for work based on Møller et al. (2016)) is likely a reasonable choice for aliphatic compounds, it is less appropriate for work with oxygenated compounds. In particular, H-bonded conformers are energetically more favorable, but tend to be more rigid, while higher-energy conformers with less or no hydrogen bonds are more loose, i.e. more entropically favorable. Thus, as can be seen in the population analysis (shown in the supporting information), conformers with energies above 2 kcal mol^{-1} are still contributing strongly to the population. In our analysis, enough conformers are included in our high-level calculations to ascertain the bulk of the population, ≥80%, is covered, and all remaining conformers are still included in the kinetic analysis using the data at the lower level of theory. Another drawback of using an energetic cut-off in the population analysis is that, with hundreds to thousands of conformers, the high number of conformers can overcome a Boltzmann weight disadvantage of one or two orders of magnitude and still provide a non-negligible contribution to the population compared to the dozen lowest-energy conformers. The impact of this can't be assessed properly without a more complete population analysis; for the case at hand, we find that at 300K over 30% of the R,R-di-HPCARP-RO_2-Ia population is

contributed by conformers over the 2 kcal mol^{-1} energy cut-off (over 50% when referenced to the 11 lowest conformers). Having most of the conformer population represented in the kinetic analysis is especially important when the temperature-dependence is examined, e.g. the contribution of the 11 lowest conformers decreases to less than 35% of the population at 400K (though obviously Møller et al. (2019) would have used a higher energy cut-off value at this temperature). As described by Møller et al. (2019), using semi-empirical methods for screening of conformers is significantly more problematic for transition states than for reactants, spreading the conformer energy range (typically 10 to 20 kcal mol^{-1} for the multi-oxygenated compounds studied here) to over more than 1000 kcal mol^{-1}. It seems unlikely that the recovered fraction of the conformers, or fraction of the population, is always sufficiently similar for minima and TS to provide reliable cancellation of error, incurring a larger uncertainty on the rate coefficient predictions and their temperature dependence. In the following section, we shortly discuss technical aspects for further improvements in MC-TST methodologies building on the benefits of both our and Møller et al. approach.

A.2 Outlook for multi-conformer methodologies

Based on the comparison between our theoretical results and that of other authors, we find that using semi-empirical methods for screening the conformers relies more on cancellation of error than has been assumed so far, at least for more complex molecules such as studied here. To our knowledge, this is the first exploratory comparison for a complex reaction system between the Møller et al. (2016) methodology based on semi-empirical screening with a kinetic analysis of a subset of the conformers on the one hand, and the all-conformer MC-TST (Vereecken and Peeters, 2003) based on DFT screening as typically performed by our research group. Hence, it is too early to properly assess the relative performance of the two MC-TST approaches. An ineffective screening method can lead to larger *a priori* uncertainties of the kinetic predictions, probably exceeding an order of magnitude when using semi-empirical methods, though the statistical nature of the sampling prevents systematic under- or over-prediction across many reactions. It is important to stress that the search of the conformer space remains a heuristic process in practice, and all practical screening methods are likely to miss some conformer in complex cases, as well as return structures that are non-existing at higher levels of theory. Furthermore, due to the large number of structures involved, it becomes more likely that e.g. erroneous structures are not removed from the populations, or that other flaws are missed by the scientist, despite extensive use of software in generating, handling, and testing all structures. Our more rigorous screening is thus also likely both a subset and superset of the true conformer pool. The larger number of conformers found, and the inclusion of all conformers in the kinetic analysis, dampens the impact to a larger extend than in the methodology of Møller et al. (2016), but this increased robustness comes at a considerable additional computational cost. Note that applying higher levels of theory afterwards on the subset of conformers obtained can't rectify shortcomings in the conformer screening.

For the reactions classes studied here, i.e. H-migration in RO_2 intermediates leading to poly-functionalized species and HOMs, there is significant interest in the chemistry of larger terpenoids. The increased computational cost of characterizing these molecules could become overwhelming, so developing efficient and accurate screening methods are critical. Despite the challenges encountered when using semi-empirical methods, the computationally more affordable methodology implemented by Møller et al. (2016) has then many uses; in particular, it remains a cost-effective method for identifying which reactions might be important or can be neglected (e.g. the α-OOH H-shift reactions or HO_2

eliminations given in Table S1), providing an order-of-magnitude estimate of the rate coefficient, and of its temperature dependence over small temperature ranges. Future work should try to identify screening methods that are computationally less costly than used in our work, yet are more reliable than semi-empirical methods in returning most conformers, or returning all low-energy conformers. A detailed numerical comparison between this work and the data in Møller et al. (2019) is outside the scope of this paper, but would be an excellent starting point in the search for reliable yet affordable screening methods. This method development would need to include quantum chemical methods such as semi-empirical, molecular mechanics, DFT, and wavefunction-based methodologies, include sampling methods such as explicit iteration over all variables, nearest-neighbor search, random walks, or Monte-Carlo sampling, and include ensemble methods, asymptotic convergence, and other quality metrics to assess the completeness of the sampling. Superimposed on this sampling problem, the traditional improvements on the prediction of energetic and rovibrational characteristics of the molecules and on the theoretical kinetic analysis, remain an important factor facing its own challenges when dealing with exceedingly large sets of conformers.

A.3 Chemistry of enol-peroxy radicals

Earlier studies have shown that unsaturated peroxy radicals can have fast ring closure reactions (Vereecken and Peeters, 2004), and this reaction class has been invoked in atmospheric models such as the OH-initiated β-pinene oxidation to explain experimentally observed nopinone and acetone yields (Kaminski et al., 2017). Similarly, H-migrations accelerated by double bonds have been proposed (Peeters et al., 2014). In contrast, the enol peroxy radicals, formed in the isoprene mechanism from Z,E'-HOO-hydroxy-allyl radicals by O_2 addition (see figure S2), are thought by Müller et al. (2019) to have no viable reaction channels competing with redissociation to an alkyl radical + O_2, implying that H-migration and ring closure reactions are negligibly slow. In this section, we perform some exploratory calculations on template enol-peroxy radicals to examine at the impact of unsaturated bonds and of –OH substitution on these two reaction classes.

Figure S2 shows the barrier heights and rate coefficients obtained for 6-membered ring closure reactions in enols. In our earlier work we only examined isoprene-derived unsaturated peroxy radicals where the –OH substituent was not attached to the double-bonded carbons, finding ring closure rates of the order of 0.3 s^{-1} at 303 K (Vereecken and Peeters, 2004). In this work, we find that the formation of α-OH cyclic peroxides significantly lowers the barriers compared to aliphatic peroxide radicals with only a spectator –OH substituent, thus increasing the reaction rates significantly (to ~10 s^{-1}). We also observe strong stereo-specificity in the calculated rates, with the Z-enols reaction being slower than E-enols. The underlying reason is the H-bond in the Z-enol reactant, which needs to break when performing the ring closure, and thus leading to a higher effective reaction barrier. Still, the rate coefficient difference between Z- and E-enols is not as large as would be expected from the difference in barrier height, as the dominant H-bonded Z-enol conformer is also much more rigid then the E-enols, leading to a lower state density for the Z-enol reactant and hence a more favorable entropic factor in the rate coefficient calculations. Figure S2 also shows the impact of a methyl group on the double bond, where we find that formation of a tertiary product radical further lowers the ring closure barrier height by 2 kcal mol^{-1}, again enhancing the reaction rate. This result is expected, confirming a traditional Evans-Polanyi correlation. Combined, we find that ring closure is accelerated by several orders of magnitude compared to the ring closure rates found in our earlier work, with ring closure rate coefficients as high as 10^3 s^{-1}.

Similar enhancement was found for H-migration reactions (see figure S2), where formation of an hydroxy-allyl-resonance stabilized radical product leads to H-migration reactions several orders of magnitude faster ($k \sim 6\times10^{-2}$ s^{-1}) than traditional, aliphatic methyl-H-abstractions which have rather slow reaction rates ($k \sim 10^{-4}$ s^{-1}) as predicted by theory and observed by experiment (Nozière and Vereecken; Sharma et al., 2010; Miyoshi, 2011; Otkjær et al., 2018). In this particular case, the H-migration rate coefficients are too low to compete against the ring closure reaction. However, the enhancement of the H-migration rates could be important for formation of oxygenates and highly oxygenated molecules (HOMs) from other compounds, where experimental evidence on HOM formation shows very high oxygen to carbon ratios, which can only be explained if all carbons in the reactant molecule are activated for oxidation. Allyl-resonance stabilization of the product radical, possibly aided by stabilizing substituents on the second radical site, could thus prove an important mechanism to enable oxygenation of otherwise mostly unreactive methyl groups in terpenoids and other atmospherically relevant compounds.

At this time, it is unclear whether the current results are directly applicable to the isoprene-derived intermediates discussed elsewhere in this work. The enol-peroxy radicals of interest there have additional oxygenated substituents, which may either enhance or reduce the reaction rate, or affect alternative loss processes such as loss of O_2. Future work will examine reactions of a wider range of enol-peroxy radicals to investigate these effects.

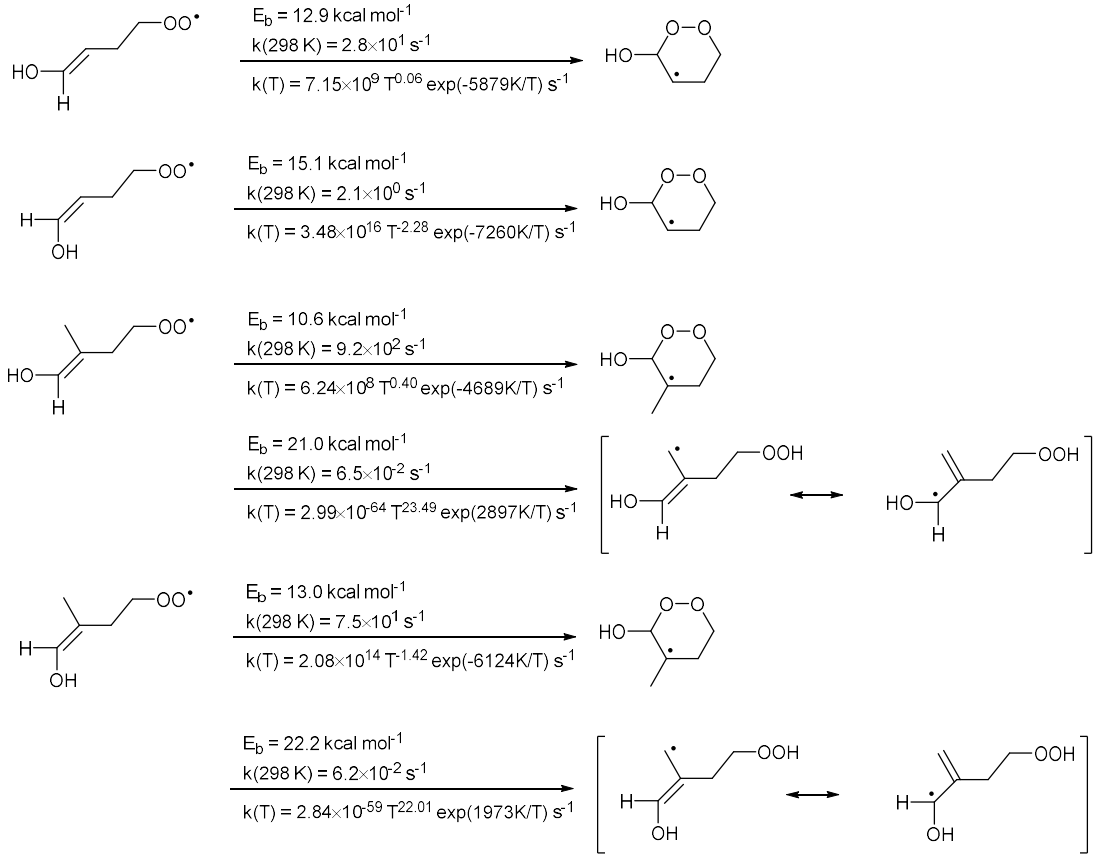

Figure S2: Barrier heights, room-temperature rate coefficients and temperature-dependent rate coefficients for ring closure and H-migration reactions in enol-peroxy radicals.

B. Kinetic models

B.1 M0 model

The M0 model is the same as the MCMv3.3.1 model but with H-shift isomerization reactions removed. To keep the number of changes as limited as possible, the removal of the isomerization reaction was implemented by removing the OH-isoprene adducts CISOPA, CISOPC, TISOPA, TISOPC that were introduced in the 2015 update to the MCM chemistry (Jenkin et al., 2015), and their equilibrium reactions. The reactions with formation of either CISOPCO2 or CISOPAO2 were likewise removed, as was the 1,5-H shift reaction as a loss path for ISOPBO2, ISOPDO2 and C524O2. To account for the resulting removal of two of the RO_2 isomers formed after reaction of isoprene with OH radicals, the yields for the remaining RO_2 radicals were scaled, accommodating the attack of the OH radicals on the isoprene carbons C2 and C3 introduced in MCMv3.3.1 (Jenkin et al., 2015). Table S2 lists all reactions affected.

Table S2 Reactions removed (in red), or modified (black) within the M0 model, compared to th MCMv3.3.1. The names of the compounds are as in the MCMv3.3.1.

Model	Reaction	Partial rate coefficient (cm^3 s^{-1})
M0	OH + C5H8 --> CISOPA	[removed]
	OH + C5H8 --> CISOPC	[removed]
	OH + C5H8 --> TISOPA	[removed]
	OH + C5H8 --> TISOPC	[removed]
	ISOPAO2 --> TISOPA	[removed]
	ISOPBO2 --> CISOPA	[removed]
	ISOPBO2 --> TISOPA	[removed]
	ISOPCO2 --> TISOPC	[removed]
	ISOPDO2 --> CISOPC	[removed]
	ISOPDO2 --> TISOPC	[removed]
	OH + C5H8 --> ISOPAO2	$2.7\times10^{-11}\times\exp(390/T)\times0.14$
	OH + C5H8 --> ISOPBO2	$2.7 \times 10^{-11}\times\exp(390/T)\times0.41$
	OH + C5H8 --> ISOPCO2	$2.7 \times 10^{-11}\times\exp(390/T)\times0.09$
	OH + C5H8 --> ISOPDO2	$2.7 \times 10^{-11}\times\exp(390/T)\times0.28$
	ISOPBO2 --> MVK + HCHO + OH	[removed]
	ISOPDO2 --> MACR + HCHO + OH	[removed]
	C524O2 --> HMACR + HCHO + OH	[removed]

B.2 M1 model

The M1 model is based on the MCMv3.3.1 model but contains:

1- The equilibrium reactions between OH-isoprene adducts and isoprene-RO_2 conformers as implemented in the Caltech mechanism (Wennberg et al., 2018).
2- A faster 1,6-H shift for the Z-δ-RO_2 combined with a higher yield of formation for di-HPCARP-RO_2 (0.6), as suggested by experimental and theoretical results (Peeters et al., 2014; Teng et al., 2017) and as described in the Caltech mechanism (Wennberg et al., 2018).
3- The rate coefficients for the aldehyde-H shift of di-HPCARP-RO_2 and product distribution as calculated from theory within this study.

Table S3 lists all reactions affected.

Table S3 Reactions modified within the M1 model, compared to th MCMv3.3.1. The names of the compounds are as in the MCMv3.3.1.

Model	Reaction	Partial rate coefficients ($cm^3\ s^{-1}$ or s^{-1})
M1	TISOPA-->ISOPAO2	0.4×10^{-12}
	TISOPA--> ISOPBO2	0.8×10^{-12}
	CISOPA-->ISOPBO2	0.8×10^{-12}
	CISOPA-->CISOPAO2	0.1×10^{-12}
	CISOPC-->CISOPCO2	0.2×10^{-12}
	CISOPC-->ISOPDO2	0.7×10^{-12}
	TISOPC-->ISOPDO2	0.7×10^{-12}
	TISOPC-->ISOPCO2	0.5×10^{-12}
	ISOPAO2-->TISOPA	$1.8\times10^{14}\times\exp(-8930/T)$
	ISOPBO2-->TISOPA	$2.2\times10^{15}\times\exp(-10355/T)$
	ISOPBO2-->CISOPA	$2.2\times10^{15}\times\exp(-10865/T)$
	CISOPAO2-->CISOPA	$1.8\times10^{14}\times\exp(-8830/T)$
	CISOPCO2-->CISOPC	$1.7\times10^{14}\times\exp(-9054/T)$
	ISOPDO2-->CISOPC	$2.5\times10^{15}\times\exp(-10890/T)$
	ISOPDO2-->TISOPC	$2.5\times10^{15}\times\exp(-11112/T)$
	ISOPCO2-->TISOPC	$2.1\times10^{14}\times\exp(-9400/T)$
	CISOPAO2-->C5HPALD1+HO2	$5.0\times10^{15}\times\exp(-12200/T)\times\exp(1\times10^{8}/T^{3})\times0.4$
	CISOPAO2-->C536O2	$5.0\times10^{15}\times\exp(-12200/T)\times\exp(1\times10^{8}/T^{3})\times0.6$
	CISOPCO2-->C5HPALD2+HO2	$2.2\times10^{9}\times\exp(-7160/T)\times\exp(1\times10^{8}/T^{3})\times0.4$
	CISOPCO2-->C537O2	$2.2\times10^{9}\times\exp(-7160/T)\times\exp(1\times10^{8}/T^{3})\times0.6$
	C536O2-->DHPMEK+CO+OH	$6.5\times10^{-53}\times T^{20.52}\times\exp(1669/T)$
	C537O2-->DHPMPAL+CO+OH	$6.5\times10^{-53}\times T^{20.52}\times\exp(1669/T)$

B.3 M2 model

The M2 model is based on the MCMv3.3.1 model but contains:

1- A faster 1,6-H shift for the Z-δ-RO_2 combined with a higher yield of formation for di-HPCARP-RO_2 (0.6), as suggested by experimental and theoretical results (Peeters et al., 2014; Teng et al., 2017) and as described in the Caltech mechanism (Wennberg et al., 2018).
2- The rate coefficients for the aldehyde-H shift of di-HPCARP-RO_2 and product distribution as calculated from theory within this study.

Table S4 lists all reactions affected.

Table S4 Reactions modified within the M2 model, compared to th MCMv3.3.1. The names of the compounds are as in the MCMv3.3.1.

Model	Reaction	Partial rate coefficients (s^{-1})
M2	CISOPAO2-->C5HPALD1+HO2	$5.0\times10^{15}\times\exp(-12200/T)\times\exp(1\times10^{8}/T^{3})\times0.4$
	CISOPAO2-->C536O2	$5.0\times10^{15}\times\exp(-12200/T)\times\exp(1\times10^{8}/T^{3})\times0.6$
	CISOPCO2-->C5HPALD2+HO2	$2.2\times10^{9}\times\exp(-7160/T)\times\exp(1\times10^{8}/T^{3})\times0.4$
	CISOPCO2-->C537O2	$2.2\times10^{9}\times\exp(-7160/T)\times\exp(1\times10^{8}/T^{3})\times0.6$
	C536O2-->DHPMEK+CO+OH	$6.5\times10^{-53}\times T^{20.52}\times\exp(1669/T)$
	C537O2-->DHPMPAL+CO+OH	$6.5\times10^{-53}\times T^{20.52}\times\exp(1669/T)$

B.4 M3 model

The M3 model is based on the MCMv3.3.1 model but contains:

1- A faster 1,6-H shift for the Z-δ-RO_2 as suggested by experimental and theoretical results (Peeters et al., 2014; Teng et al., 2017) and as described in the Caltech mechanism (Wennberg et al., 2018).
2- A larger yield for HPALD as described in the study by Berndt et al. (2019)
3- The rate coefficients for the aldehyde-H shift of di-HPCARP-RO_2 and product distribution as calculated from theory within this study.

Table S5 lists all reactions affected.

Table S5 Reactions modified within the M3 model, compared to th MCMv3.3.1. The names of the compounds are as in the MCMv3.3.1.

Model	Reaction	Partial rate coefficients (s^{-1})
M3	CISOPAO2-->C5HPALD1+HO2	$5.0\times10^{15}\times\exp(-12200/T)\times\exp(1\times10^{8}/T^{3})\times0.75$
	CISOPAO2-->C536O2	$5.0\times10^{15}\times\exp(-12200/T)\times\exp(1\times10^{8}/T^{3})\times0.25$
	CISOPCO2-->C5HPALD2+HO2	$2.2\times10^{9}\times\exp(-7160/T)\times\exp(1\times10^{8}/T^{3})\times0.75$
	CISOPCO2-->C537O2	$2.2\times10^{9}\times\exp(-7160/T)\times\exp(1\times10^{8}/T^{3})\times0.25$
	C536O2-->DHPMEK+CO+OH	$6.5\times10^{-53}\times T^{20.52}\times\exp(1669/T)$
	C537O2-->DHPMPAL+CO+OH	$6.5\times10^{-53}\times T^{20.52}\times\exp(1669/T)$

C. Modelled OH regeneration efficiency (RE)

The aldehyde-H shift includes the isomerization reaction of the di-HPCARP-RO_2 (C536O2 and C537O2) formed after the isomerization of the Z-*δ*-RO_2, combined with the OH radical which is directly recycled from the products of the aldehyde-H shift (dihydroperoxy carbonyl compounds, DHPMEK and DHPMPAL). In addition, the isomerization of the RO_2 which originates from OH reaction with MACR (MACRO2) is included (Table S6).

Table S6. Reaction paths forming OH radicals included in the modelled OH regeneration efficiency, with their label as used in figure 7. The names of the compounds are as in the MCMv3.3.1.

Reaction label	Reaction paths included
HONO + *hv*	HONO + *hv*
O_3 + *hv*	O_3 + *hv*
HO_2+ O_3	HO_2+ O_3
HO_2 + NO	HO_2 + NO
1,5-H shift	ISOPBO2 and ISOPDO2
HPALD + *hv*	C5HPALD1+ C5HPALD2+ C5PACALD1+ C5PACALD2 + *hv*
Aldehyde-H shift	C536O2, C537O2, DHPMEK, DHPMPAL, MACRO2

D. Global model

The ECHAM/MESSy Atmospheric Chemistry (EMAC) (Jöckel et al., 2010) model was used to investigate the global impact of changes in the isomerization of the isoprene chemistry. In this study, two simulations were performed using the Mainz Organic Mechanism (MOM) (Sander et al., 2019). The first simulation served as a reference and the second one included changes as discussed in this study. In the reference simulation, no 1,6-H shift and aldehyde-H shift isomerization in the isoprene chemistry were included (comparable to the no-H shift model). The second simulation is comparable to the M2 model and includes isomerization reactions (1,5-, 1,6- and aldehyde –H shift) using a 0.4 yield for HPALD and 0.6 yield for di-HPCARP-RO_2 from the 1,6-H shift. In addition, traditional RO_2 chemistry was included for HPALD and di-HPCARP as used in the MCMv3.3.1. For both simulations, the reaction rates adapted from LIM1 (Peeters et al., 2014) for the equilibrium reactions between OH-isoprene adducts and isoprene-RO_2 conformers were used. Finally, a third simulation was run where the yield of HPALD was set to 0.75, comparable to model M3. The relevant reactions are listed in table S7, while the impact on the OH concentrations is illustrated in figure S3.

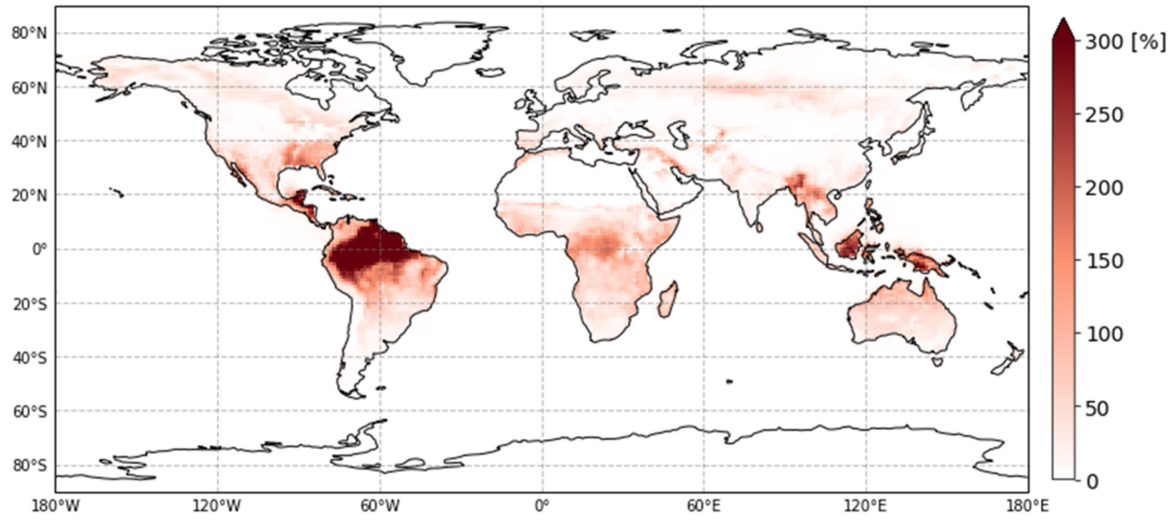

Figure S3. Relative increase of the global ground-level concentration of OH radicals. The implementation of a fast rate coefficient for the 1,6-H shift together with the inclusion of the aldehyde-H shift results in an increase of more than a factor of 3 for the OH radical concentrations in regions with large concentrations of isoprene and low NO, when compared to a model without isomerization reactions.

Table S7. Changes to the MOM mechanism used in this study to assess the global impact of isomerisation reaction in the isoprene chemistry. The names of the compounds are as in the original MOM mechanism, whereas newly added compounds are labeled as in the MCMv3.3.1.

Reaction	(Partial) Rate coefficients ($cm^3\ s^{-1}$ or s^{-1})
LISOPACO2-->C536O2	5.47 x 10^{15} x EXP(-12200/T) x EXP(1.D8/T^3) x 0.6
LISOPACO2-->ZCODC23DBCOOH+HO2	5.47 x 10^{15} x EXP(-12200/T) x EXP(1.D8/T^3))x 0.4
LDISOPACO2-->C537O2	5.47 x 10^{15} x EXP(-12200/T) x EXP(1.D8/T^3) x 0.6
LDISOPACO2-->ZCODC23DBCOOH+HO2	5.47 x 10^{15} x EXP(-12200/T) x EXP(1.D8/T^3) x 0.4
C536O2+HO2-->C536OOH+O2	2.91 x 10^{-13} x EXP(1300/T)*0.706
C536O2+NO-->C536O+NO2	2.54 x 10^{-12} x EXP(360./T)
C536O2+NO3-->C536O+NO2	2.50 x 10^{-12}
C536O2-->C536O	9.20 x 10^{-14} x RO2
C536O2-->DHPMEK+CO+OH	$6.52\times10^{-53}\times T^{20.52}\times\exp(1669/T)$
C537O2+HO2-->C537OOH+O2	2.91 x 10^{-13} x EXP(1300/T)*0.706
C537O2+NO-->C537O+NO2	2.54 x 10^{-12} x EXP(360./T)
C537O2+NO3-->C537O+NO2	2.50 x 10^{-12}
C537O2-->C537O	8.80 x 10^{-13} x RO2
C537O2-->DHPMPAL+CO+OH	$6.52\times10^{-53}\times T^{20.52}\times\exp(1669/T)$
C536OOH+OH-->DHPMEK+CO+OH	6.60 x 10^{-11}
C536O-->MGLYOX+HOOCH2CHO+OH	1.00 x 10^{6}
C537OOH+OH-->DHPMPAL+CO+OH	5.64 x 10^{-11}
C537O-->GLYOX+HYPERACET+OH	1.00 x 10^{6}
DHPMEK+OH-->BIACETOOH+OH+H2O	2.92 x 10^{-11} x 0.56
DHPMEK+OH-->C4CO2OOH+OH+H2O	2.92 x 10^{-11} x 0.44
DHPMPAL+OH-->C3MDIALOOH+OH+H2O	3.77 x 10^{-11} x 0.32
DHPMPAL+OH-->HYPERACET+CO+OH+ H2O	3.77 x 10^{-11} x 0.68
C3MDIALOOH+OH-->C3MDIALO2+H2O	1.35 x 10^{-10}
C4CO2OOH+OH-->CO23C3CHO+OH+H2O	7.83 x 10^{-11}
C4CO2O+O2-->GLYOX+CH3CO3	1.00 x 10^{6} x 0.5
C4CO2O+O2-->MGLYOX+HO2+CO	1.00 x 10^{6} x 0.5
C3MDIALO+O2-->MGLYOX+CO+HO2	1.00 x 10^{6}
C536OOH+hv-->C3MDIALOOH+HCHO+OH+OH	jx(ip_CH3OOH)
C536OOH+hv-->DHPMEK+CO+OH+HO2	jx(ip_IPRCHO2HCO)
C536OOH+hv-->MGLYOX+HOOCH2CHO+OH+OH	jx(ip_CH3OOH)*2
C537OOH+hv-->C4CO2OOH+HCHO+OH+OH	jx(ip_CH3OOH)
C537OOH+hv-->DHPMPAL+CO+OH+HO2	jx(ip_IPRCHO2HCO)
C537OOH+hv-->GLYOX+HYPERACET+OH+OH	jx(ip_CH3OOH)*2
DHPMEK+hv-->CH3CO3+HOOCH2CHO+OH	jx(ip_CH3OOH)+ jx(ip_CHOH)* 0.42
DHPMEK+hv-->MGLYOX+HCHO+OH+OH	jx(ip_CH3OOH)
DHPMPAL+hv-->C3MDIALOOH+OH	jx(ip_CH3OOH)
DHPMPAL+hv-->HYPERACET+OH+CO+HO2	jx(ip_C3H7CHO2HCO)
DHPMPAL+hv-->MGLYOX+OH+HCHO+OH	jx(ip_CH3OOH)
C3MDIALOOH+hv-->C3MDIALO+OH	jx(ip_CH3OOH)
C3MDIALOOH+hv-->MGLYOX+OH+HO2+CO	jx(ip_IPRCHO2HCO)*2
C4CO2OOH+hv-->C4CO2O+OH	jx(ip_CH3OOH)
C4CO2OOH+hv-->CH3CO3+GLYOX+OH	jx(ip_CHOH)* 0.42
C4CO2OOH+hv-->HO2+CO+MGLYOX+OH	jx(ip_IPRCHO2HCO)

D. Additional tables and figures

Table S8. Rate coefficients for the addition of O_2 to OH-isoprene adducts, and for re-dissociation of isoprene-RO_2 (Fig. 1). The rate coefficients for the oxygen additions (kf) are in cm^3 s^{-1} and are typically temperature independent. The rate coefficient for the re-dissociations (kr) are in s^{-1}.

	LIM1(Peeters et al., 2014)	MCMv3.3.1 (Jenkin et al., 2015)	Caltech (Wennberg et al., 2018)
kf1	$0.5\times10^{-12}\times\exp(-480/T)$ -	$2.5\times10^{-12}\times\exp(-480/T)$	0.4×10^{-12}
kf2	0.6×10^{-12}	3.0×10^{-12}	0.8×10^{-12}
kf3	0.6×10^{-12}	3.0×10^{-12}	0.8×10^{-12}
kf4	0.7×10^{-12}	3.5×10^{-12}	0.1×10^{-12}
kf5	0.4×10^{-12}	2.0×10^{-12}	0.2×10^{-12}
kf6	0.7×10^{-12}	3.5×10^{-12}	0.7×10^{-12}
kf7	0.7×10^{-12}	3.5×10^{-12}	0.7×10^{-12}
kf8	$0.5\times10^{-12}\times\exp(-480/T)$	$2.5\times10^{-12}\times\exp(-480/T)$	0.5×10^{-12}
kr1	$5.7\times10^{13}\times\exp(-9028/T)$	$2.9\times10^{14}\times\exp(-9028/T)$	$1.8\times10^{14}\times\exp(-8930/T)$
kr2	$1.7\times10^{15}\times\exp(-10743/T)$	$8.5\times10^{15}\times\exp(-10743/T)$	$2.2\times10^{15}\times\exp(-10355/T)$
kr3	$1.7\times10^{15}\times\exp(-11322/T)$	$8.6\times10^{15}\times\exp(-11322/T)$	$2.2\times10^{15}\times\exp(-10865/T)$
kr4	$1.0\times10^{15}\times\exp(-9838/T)$	$5.2\times10^{15}\times\exp(-9838/T)$	$1.8\times10^{14}\times\exp(-8830/T)$
kr5	$6.1\times10^{14}\times\exp(-10254/T)$	$3.1\times10^{15}\times\exp(-10254/T)$	$1.7\times10^{14}\times\exp(-9054/T)$
kr6	$2.1\times10^{15}\times\exp(-11705/T)$	$1.1\times10^{16}\times\exp(-11705/T)$	$2.5\times10^{15}\times\exp(-10890/T)$
kr7	$2.1\times10^{15}\times\exp(-11569/T)$	$1.1\times10^{16}\times\exp(-11569/T)$	$2.5\times10^{15}\times\exp(-11112/T)$
kr8	$4.2\times10^{13}\times\exp(-9984/T)$	$2.1\times10^{14}\times\exp(-9984/T)$	$2.1\times10^{14}\times\exp(-9400/T)$

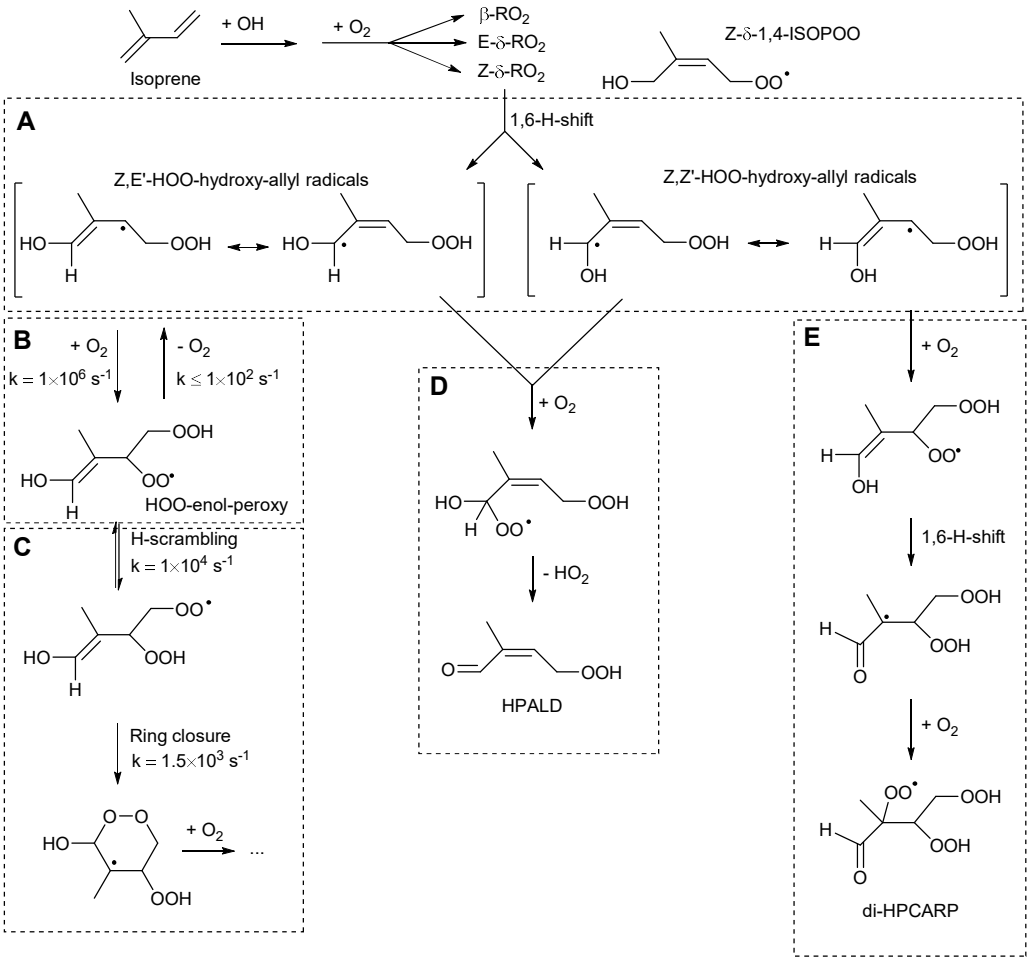

Figure S4: Reaction scheme detailing the reaction steps affecting the HPALD vrs. di-HPCARP yields. The submechanism in the labeled boxes A through E are discussed in the text.

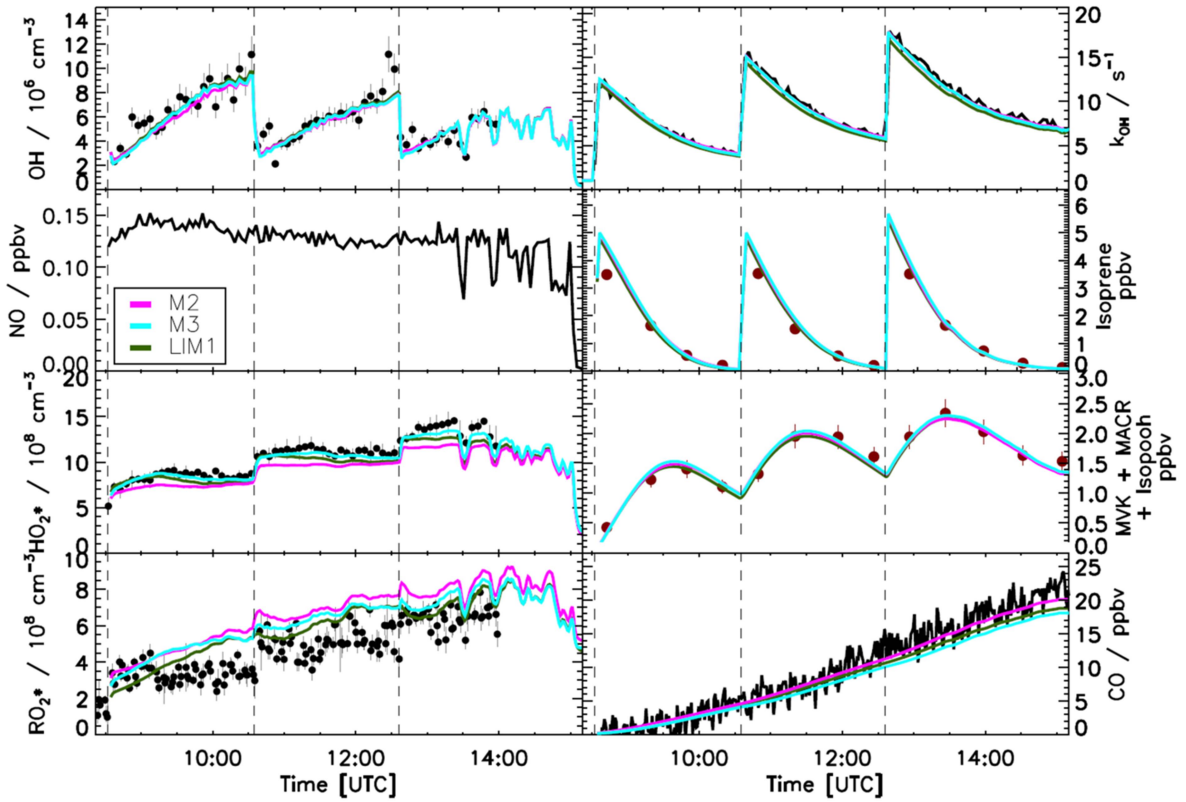

Figure S5. Comparison of modelled and measured trace gases for an experiment with NO < 0.2 ppbv. Measured time series of radicals and OH reactivity (LIF), isoprene and MVK+MACR+ISOPOOHs (GC) and CO (Picarro) are compared to model calculations. Vertical dashed lines indicate the times when isoprene was injected. Good agreement is observed when using M2, M3 or LIM1 (Table 2). Error bars represent 1 σ standard deviation.

References

Alecu, I. M., Zheng, J., Zhao, Y., and Truhlar, D. G.: Computational Thermochemistry: Scale Factor Databases and Scale Factors for Vibrational Frequencies Obtained from Electronic Model Chemistries, Journal of Chemical Theory and Computation, 6, 2872-2887, doi:10.1021/ct100326h, 2010.

Bao, J. L., Zheng, J., Alecu, I. M., Lynch, B. J., Zhao, Y., and Truhlar, D. G.: Database of Frequency Scale Factors for Electronic Model Chemistries (Version 3 Beta 2), 2017.

Berndt, T., Hyttinen, N., Herrmann, H., and Hansel, A.: First oxidation products from the reaction of hydroxyl radicals with isoprene for pristine environmental conditions, Comm. Chem., 2, 21, doi:10.1038/s42004-019-0120-9, 2019.

Dunning, T. H.: Gaussian basis sets for use in correlated molecular calculations. I. The atoms boron through neon and hydrogen, The Journal of Chemical Physics, 90, 1007-1023, doi:10.1063/1.456153, 1989.

Jenkin, M. E., Young, J. C., and Rickard, A. R.: The MCM v3.3.1 degradation scheme for isoprene, Atmos Chem Phys, 15, 11433-11459, doi:10.5194/acp-15-11433-2015, 2015.

Jöckel, P., Kerkweg, A., Pozzer, A., Sander, R., Tost, H., Riede, H., Baumgaertner, A., Gromov, S., and Kern, B.: Development cycle 2 of the Modular Earth Submodel System (MESSy2), Geosci. Model Dev., 3, 717-752, doi:10.5194/gmd-3-717-2010, 2010.

Kaminski, M., Fuchs, H., Acir, I. H., Bohn, B., Brauers, T., Dorn, H. P., Häseler, R., Hofzumahaus, A., Li, X., Lutz, A., Nehr, S., Rohrer, F., Tillmann, R., Vereecken, L., Wegener, R., and Wahner, A.: Investigation of the β-pinene photooxidation by OH in the atmosphere simulation chamber SAPHIR, Atmos. Chem. Phys., 17, 6631-6650, doi:10.5194/acp-17-6631-2017, 2017.

Miyoshi, A.: Systematic computational study on the unimolecular reactions of alkylperoxy (RO_2), hydroperoxyalkyl (QOOH), and hydroperoxyalkylperoxy (O_2QOOH) radicals, J. Phys. Chem. A, 115, 3301-3325, doi:10.1021/jp112152n, 2011.

Møller, K. H., Otkjær, R. V., Hyttinen, N., Kurtén, T., and Kjaergaard, H. G.: Cost-Effective Implementation of Multiconformer Transition State Theory for Peroxy Radical Hydrogen Shift Reactions, J Phys Chem A, 120, 10072-10087, doi:10.1021/acs.jpca.6b09370, 2016.

Møller, K. H., Bates, K. H., and Kjaergaard, H. G.: The importance of peroxy radical hydrogen-shift reactions in atmospheric isoprene oxidation, J. Phys. Chem. A, 123, 920-932, doi:10.1021/acs.jpca.8b10432, 2019.

Müller, J. F., Stavrakou, T., and Peeters, J.: Chemistry and deposition in the Model of Atmospheric composition at Global and Regional scales using Inversion Techniques for Trace gas Emissions (MAGRITTE v1.1) – Part 1: Chemical mechanism, Geosci. Model Dev., 12, 2307-2356, doi:10.5194/gmd-12-2307-2019, 2019.

Nozière, B., and Vereecken, L.: Direct Observation of Aliphatic Peroxy Radical Autoxidation and Water Effects: An Experimental and Theoretical Study, Angewandte Chemie International Edition, 0, doi:10.1002/anie.201907981.

Ocaña, A. J., Blázquez, S., Potapov, A., Ballesteros, B., Canosa, A., Antiñolo, M., Vereecken, L., Albaladejo, J., and Jiménez, E.: Gas-phase reactivity of CH₃OH toward OH at interstellar temperatures (11.7–177.5 K): experimental and theoretical study, Phys Chem Chem Phys, DOI:-10.1039/C1039CP00439D, doi:10.1039/C9CP00439D, 2019.

Otkjær, R. V., Jakobsen, H. H., Tram, C. M., and Kjaergaard, H. G.: Calculated Hydrogen Shift Rate Constants in Substituted Alkyl Peroxy Radicals, The Journal of Physical Chemistry A, 122, 8665-8673, doi:10.1021/acs.jpca.8b06223, 2018.

Peeters, J., Müller, J.-F., Stavrakou, T., and Nguyen, V. S.: Hydroxyl radical recycling in isoprene oxidation driven by hydrogen bonding and hydrogen tunneling: the upgraded LIM1 mechanism, J. Phys. Chem. A, doi:10.1021/jp5033146, 2014.

Purvis, G. D., and Bartlett, R. J.: A full coupled-cluster singles and doubles model: The inclusion of disconnected triples, The Journal of Chemical Physics, 76, 1910, doi:10.1063/1.443164, 1982.

Sander, R., Baumgaertner, A., Cabrera-Perez, D., Frank, F., Gromov, S., Grooß, J. U., Harder, H., Huijnen, V., Jöckel, P., Karydis, V. A., Niemeyer, K. E., Pozzer, A., Riede, H., Schultz, M. G., Taraborrelli, D., and Tauer, S.: The community atmospheric chemistry box model CAABA/MECCA-4.0, Geosci. Model Dev., 12, 1365-1385, doi:10.5194/gmd-12-1365-2019, 2019.

Sharma, S., Raman, S., and Green, W. H.: Intramolecular Hydrogen Migration in Alkylperoxy and Hydroperoxyalkylperoxy Radicals: Accurate Treatment of Hindered Rotors, The Journal of Physical Chemistry A, 114, 5689-5701, doi:10.1021/jp9098792, 2010.

Teng, A. P., Crounse, J. D., and Wennberg, P. O.: Isoprene peroxy radical dynamics, J Am Chem Soc, 139, 5367-5377, doi:10.1021/jacs.6b12838, 2017.

Vereecken, L., and Peeters, J.: The 1,5-H-shift in 1-butoxy: A case study in the rigorous implementation of transition state theory for a multirotamer system, J. Chem. Phys., 119, 5159-5170, doi:10.1063/1.1597479, 2003.

Vereecken, L., and Peeters, J.: Nontraditional (Per)oxy Ring-Closure Paths in the Atmospheric Oxidation of Isoprene and Monoterpenes, The Journal of Physical Chemistry A, 108, 5197-5204, doi:10.1021/jp049219g, 2004.

Wang, S., Riva, M., Yan, C., Ehn, M., and Wang, L.: Primary formation of highly oxidized multifunctional products in the OH-Initiated oxidation of Isoprene: a combined theoretical and experimental study, Environ Sci Technol, 52, 12255-12264, doi:10.1021/acs.est.8b02783, 2018.

Wennberg, P. O., Bates, K. H., Crounse, J. D., Dodson, L. G., McVay, R. C., Mertens, L. A., Nguyen, T. B., Praske, E., Schwantes, R. H., Smarte, M. D., St Clair, J. M., Teng, A. P., Zhang, X., and Seinfeld, J. H.: Gas-phase reactions of isoprene and its major oxidation products, Chem. Rev., doi:10.1021/acs.chemrev.7b00439, 2018.

Zhao, Y., and Truhlar, D. G.: The M06 suite of density functionals for main group thermochemistry, thermochemical kinetics, noncovalent interactions, excited states, and transition elements: two new functionals and systematic testing of four M06-class functionals and 12 other functionals, Theoretical Chemistry Accounts, 120, 215-241, doi:10.1007/s00214-007-0310-x, 2008.